# Reports

## Spatially Resolved Observation of Supercurrents Across Grain Boundaries in YBaCuO Films

J. MANNHART, R. GROSS, K. HIPLER, R. P. HUEBENER, C. C. TSUEI, D. DIMOS, P. CHAUDHARI

**Spatially resolved resistivity measurements of current transport across individual grain boundaries have been made on superconducting $YBa_2Cu_3O_7$. These experiments were done by low-temperature scanning electron microscopy with a resolution of 1 to 2 micrometers, and they show directly the limitation of the critical current density caused by grain boundaries in $YBa_2Cu_3O_7$. Furthermore, complex spatial patterns of the current transport across grain boundaries were observed. These patterns reflect self-excited resonances of the grain boundaries and are closely correlated to the unexplained "sub–gap structure" in the current-voltage characteristics of polycrystalline $YBa_2Cu_3O_7$.**

A DETAILED UNDERSTANDING OF THE electronic properties of the grain boundaries in superconducting $YBa_2Cu_3O_7$ is important both for fundamental reasons and for possible applications of this superconductor. The fact that the critical current density of polycrystalline $YBa_2Cu_3O_7$ is limited by the grain boundaries (*1*) represents a particularly crucial point. In past experimental studies of individual grain boundaries, only the spatially averaged behavior of the grain boundaries has been investigated, leaving important questions unresolved. For this reason, we have studied the spatial behavior of supercurrents flowing across grain boundaries in $YBa_2Cu_3O_7$ films by low-temperature scanning electron microscopy (LTSEM) (*2*). This work has confirmed the limitation of the critical current density of polycrystalline $YBa_2Cu_3O_7$ films caused by the grain boundaries. Further, two-dimensional structures caused by the supercurrent flowing across the grain boundaries have been found; these structures are closely linked to the so far unexplained "sub–gap structures" (*1, 3, 4*) in the current-voltage characteristics (IVC) of the boundaries. We conclude that these sub–gap structures are caused by self-induced, electronic resonances and do not reflect any feature of the quasi-particle spectrum of the superconductor.

The sample investigated by LTSEM was a thin film bicrystal of $YBa_2Cu_3O_7$. In other words, it consisted of two grains that formed one grain boundary. The film, which was 0.5 μm thick and oriented with the surface normal to the *c* axis, had a nominally symmetric grain boundary with a tilt of 38° and was grown epitaxially on a $SrTiO_3$ bicrystal as previously described (*5*). Superconducting lines, about 20 μm wide and 100 μm long, were patterned into the film by ablation with a focused laser beam (*6*). Two of these lines straddled the grain boundary, four lines were located in the grain. The transport properties of this sample were typical within a set of about 30 samples. For the LTSEM studies, the sample was mounted onto a temperature-controlled cooling stage and biased with a constant current $I$, as shown schematically in Fig. 1. As the pulsed electron beam (energy ≃ 26 keV, current ≃ $10^{-9}$ A, repetition rate = 10 kHz) was scanned over the surface of the superconducting sample, the beam-induced voltage change $\delta V$ of the voltage $V$ across the sample was measured with a phase-sensitive detection (lock-in) technique as a function of the position of the electron beam focus. The beam-induced voltage signal $\delta V$ was then used to control the brightness of the SEM video screen.

Figure 2 shows the result of such a measurement for a superconducting line straddling the grain boundary. The measurements shown in Fig. 2, b through d, were taken at 86.3 K for three different bias currents. Dark regions represent areas where $\delta V$ was zero. In the bright areas, $\delta V$ was about 1 μV. If the sample was biased with a current $I < 50$ μA, no voltage signal was detected for any location of the electron beam. However, if $I$ was increased above 50 μA, a finite voltage signal was obtained for a narrow region along the grain boundary (Fig. 2b). For currents $I > 0.8$ mA and $> 3$ mA the right and the left grain produced a voltage signal, respectively (Fig. 2, c and d).

The results shown in Fig. 2 can be interpreted as follows. A nonzero voltage $V$ along a superconducting line is obtained only if a complete cross section $A_0$ of the line is in the resistive state. If the electron beam is focused on a spot within $A_0$, it

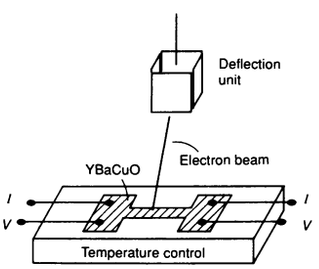


**Fig. 1.** Sketch of the LTSEM setup.

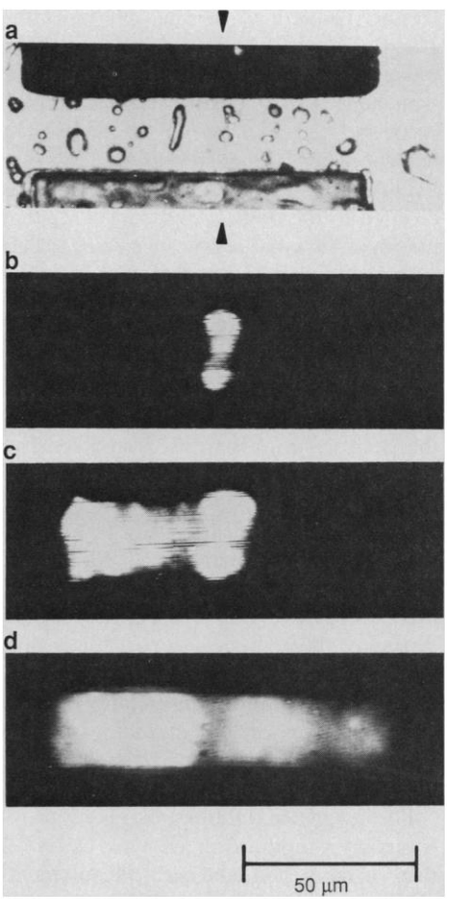


**Fig. 2.** LTSEM measurement of a YBaCuO line straddling one grain boundary; $T = 86.3$ K. (**a**) An optical micrograph of the line. The location of the grain boundary is marked by the triangles. The dark regions at the top and at the bottom are the laser-ablated areas. (**b–d**) The voltage response $\delta V$ (bright = $\delta V > 0$) of the line for three different bias currents: (b) 0.56 mA, (c) 1.9 mA, and (d) 32 mA.

J. Mannhart, R. Gross, K. Hipler, R. P. Huebener, Physikalisches Institut, Lehrstuhl Experimentalphysik II, Universität Tübingen, D-7400 Tübingen, Federal Republic of Germany.
C. C. Tsuei, D. Dimos, P. Chaudhari, IBM Research Division, T. J. Watson Research Center, Yorktown Heights, NY 10598.

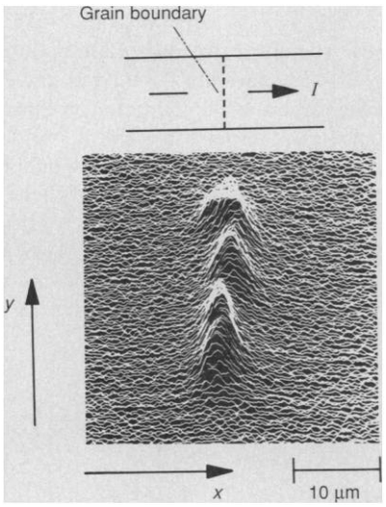


**Fig. 3.** Voltage image $\delta V(x,y)$ of the grain boundary taken with a bias current of 39 mA at 14 K.

increases the resistance $R_f$ of the superconductor within a volume $A_f$ with radius $r$ around the beam focus. This resistance increase is caused by thermal effects of the electron beam; therefore, $r$ is given by the thermal properties of the sample and is estimated to be $\simeq 1$ μm (*7*). The electron beam–induced increase of $R_f$ leads to a reduction $\delta I$ of the current $I$ across $A_f$. Because the sample is current-biased, $\delta I$ is diverted to the unirradiated part of $A_0$ that has the differential resistance $dV/dI(I)$. This leads to a signal $\delta V = \delta I\ dV/dI(I)$. On the other hand, if $A_0$ is in the zero resistance state, no voltage signal can be obtained, if $I$ is smaller than the critical current of $A_0 - A_f$. In short, an electron beam–induced voltage is generally expected only if the electron beam is focused on a resistive area of the sample. A detailed discussion of the signal generation in this type of experiments has been published (*7*).

Figure 2 demonstrates that, with increasing current density, first the grain boundary becomes resistive; that is, the critical current density of the grain boundary is lower than that of the grains. This result directly confirms earlier measurements (*1*), in which the critical currents of lines straddling a grain boundary have been compared to the critical currents of lines inside grains.

For quantitative studies, observations recorded by $y$ modulation are more useful (*2*) than brightness-modulated measurements like the one shown in Fig. 2. Therefore, in Fig. 3 a $y$-modulated measurement of the same grain boundary is shown. Here, for a series of horizontal line scans, $\delta V$ has been added in the $y$ direction to the position of the electron beam. The apparent width of the signal-generating area in Fig. 3 (along the $x$ direction) corresponds to the spatial resolution of the imaging technique, limited by the thermal healing length $r$. This technique gives an upper limit for the effective grain boundary width of about 2 μm. The region in the middle of the bridge with a small signal $\delta V$ is an area where a precipitate can be optically observed on the film surface. The small value of $\delta V$ at this coordinate may be a consequence of the reduction of the film thickness by the precipitate, which leads to a reduced $\delta I$ and thereby to a smaller $\delta V$.

The LTSEM technique was also applied to the study of the so far unexplained sub–gap structures in the IVC of grain boundaries. These features have been suspected of reflecting intrinsic properties of high-temperature ($T_c$) superconductors and have generated considerable interest (*1, 3, 4*). These sub–gap structures can be seen clearly in the $dV/dI(V)$ characteristics of the 38°-tilt boundary for voltages below 500 μV (Fig. 4a). Such features have been found at all grain boundaries that we have investigated, however only rarely with such periodicity. Similar features have also been reported from transport measurements of polycrystalline $YBa_2Cu_3O_7$ samples (*3*). We have found that these sub–gap features correspond directly to complex spatial patterns of the current flow across the boundary. The peaks in the $dV/dI(V)$ characteristic correlate with spatial modes of $\delta V$ (Fig. 4, b and c). A close connection between the sub–gap structures and the spatial structures was demonstrated by a magnetic field pulse (100 G, 5 s) oriented perpendicular to the film surface, which dramatically changed both the sub–gap structure and the spatial patterns but did not affect the overall IVC. After the pulse, the $dV/dI(V)$ characteristic was flattened out, a substantial peak was observed only at 50 μV, and for all voltages a rather weak and uniform voltage response was obtained.

These results show that the sub–gap structure is not related to intrinsic properties of the superconductor such as the quasiparticle spectrum but is most likely a result of spatial electronic excitations of the grain boundaries. These excitations might consist of self-excited resonances between the high-frequency resonance mode of the grain boundary region and the Josephson frequency resulting from the voltage across the boundary. Such resonances are expected at voltages (*8*)

$$V = n\frac{hc}{qb}\left(\frac{d}{\epsilon_r^{eff}\ell}\right)^{1/2};$$

$$(n = \ldots 1/3, 1/2, 1, 2, 3 \ldots) \qquad (1)$$

where $c$ is the vacuum speed of light, $h$ is Planck's constant, $q$ is the charge of the

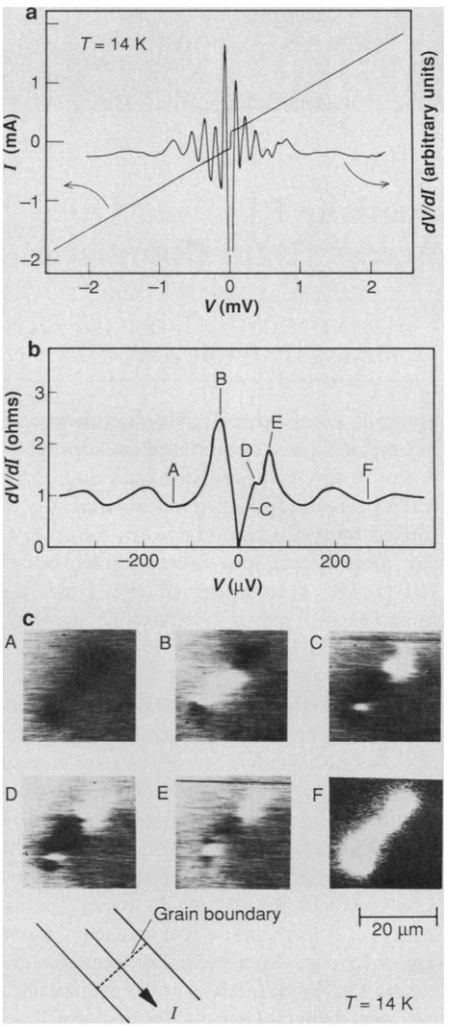


**Fig. 4.** (**a** and **b**) $I(V)$ and $dV/dI(V)$ characteristics of the grain boundary. (**c**) Voltage image of the grain boundary area taken at the bias points shown in (b).

Cooper pairs, $b$ is the length of the resonance cavity, $d$ is the thickness of the boundary layer, and $\ell = d + 2\lambda_\ell$, where $\lambda_l$ is the London penetration depth. Although these parameters are well known [$d \simeq 10$ Å[6], $\lambda_\ell \simeq 1500$ Å (*9*), $b \simeq 4$ μm], the effective dielectric constant $\epsilon_r^{eff}$ of the $YBa_2Cu_3O_7$ grain boundary on $SrTiO_3$ can only be roughly estimated. Using for the dielectric constant of $SrTiO_3$ $\epsilon_r$ (2 K) $\simeq$ 20,000 (*10*), we estimate $\epsilon_r^{eff}$ to be $\simeq$5000 for the grain boundary. If we use these values, Eq. 1 yields a resonance voltage $V_{res} \simeq 100$ μV, which indeed lies in the range of the sub–gap structures.


REFERENCES AND NOTES

1. P. Chaudhari *et al.*, *Phys. Rev. Lett.* **60**, 1653 (1988).
2. R. P. Huebener, *Adv. Electron. Electron Phys.* **70**, 1 (1988).
3. K. Iida *et al.*, *Proc. Mater. Res. Soc. Symp. High-$T_c$ Mater.* **99**, 765 (1987).
4. J. Kuznik, M. Odehnal, S. Safrata, *J. Low Temp.*

*Phys.* **72**, 283 (1988).
5. D. Dimos *et al.*, *Phys. Rev. Lett.* **61**, 219 (1988).
6. J. Mannhart *et al.*, *Appl. Phys. Lett.* **52**, 1271 (1988).
7. R. Gross *et al.*, *IEEE Trans. Magn.* **25**, 2250 (1989).
8. A. Barone and G. Paterno, *Physics and Applications of the Josephson Effect* (Wiley, New York, 1982).
9. A. T. Fiory *et al.*, *Phys. Rev. Lett.* **61**, 1419 (1988).
10. H. Gränicher, *Helv. Phys. Acta* **29**, 211 (1956).
11. We thank J. Berosh, D. R. Clarke, J. Hagerhorst, J. Lacey, M. M. Oprysko, and T. M. Shaw for support. Part of this work was supported by a grant of the Bundesministerium für Forschung und Technology (Projekt 13N5482).

3 May 1989; accepted 20 June 1989

# Prediction of New Low Compressibility Solids

AMY Y. LIU AND MARVIN L. COHEN

**An empirical model and an ab initio calculation of the bulk moduli for covalent solids are used to suggest possible new hard materials. The empirical model indicates that hypothetical covalent solids formed between carbon and nitrogen are good candidates for extreme hardness. A prototype system is chosen and a first principles pseudopotential total energy calculation on the system is performed. The results are consistent with the empirical model and show that materials like the prototype can have bulk moduli comparable to or greater than diamond. It may be possible to synthesize such materials in the laboratory.**

HARDNESS (*1*) IS A COMPLEX PROPerty related to the extent to which solids resist both elastic and plastic deformation. For materials with defects, hardness can be limited by many factors including point defects, dislocations, and macroscopic defects. On the microscopic level, for ideal systems, hardness is determined by the bulk modulus, which in turn depends on the nature of the chemical bonding. It is the strength and compressibility of the bond that plays the primary role in a solid's ability to resist deformation. The largest bulk moduli are found in covalently bonded materials. Diamond, which has the largest bulk modulus (4.43 Mbar), is also the hardest known solid. A theory of the bulk moduli of covalent solids is therefore useful for suggesting schemes to increase hardness.

An empirical model for the bulk moduli of covalent solids was developed (*2*) with scaling arguments based on the Phillips–Van Vechten scheme (*3*) for characterizing the covalent and ionic nature of tetrahedral solids by means of their spectral properties. For purely covalent solids such as C and Si, the bulk modulus scales as the average homopolar energy gap in the reflectivity spectrum divided by the volume of the bond charge. This leads to the bulk modulus varying as $d^{-3.5}$, where $d$ is the bond length. For the zinc blendes, an additional empirical term is added to account for the depletion of bond charge with increasing ionicity. The resulting scaling relation is

$$B = \frac{(19.71 - 2.20\lambda)}{d^{3.5}} \qquad (1)$$

where $B$ is the bulk modulus in megabars, $d$ is in angstroms, and $\lambda$ is a measure of the ionicity of the compound. For the homopolar semiconductors (group IV), $\lambda = 0$, while for the heteropolar III-V and II-VI zinc blende solids, $\lambda = 1$ and 2, respectively. Similar analytic relations between the bulk modulus and lattice constant have been obtained for the group IV and III-V semiconductors by means of first principles methods based on a pseudopotential scheme (*4*).

The scaling law given by Eq. 1 successfully describes the diamond and zinc blende semiconductors, giving results for the bulk moduli within a few percent. This is comparable in accuracy to first principles calculations (*5*) that require extensive supercomputer time. Equation 1 is also useful for illustrating trends in these materials. For example, to achieve a large bulk modulus, two properties are needed: low ionicity and short bond length. In the past, there was speculation that cubic BN might be harder than diamond. Interpolation of empirical relations for the elastic constants (*6*) led to an estimate of the bulk modulus of BN in the range of 4.65 Mbar. In contrast, because both the bond length and ionicity are larger in BN than in diamond, Eq. 1 predicts that BN should have a smaller bulk modulus than diamond. With $\lambda = 1$ and $d = 1.56$ Å, the scaling law yields $B = 3.67$ Mbar for BN. A recent measurement (*7*) of the bulk modulus of BN yields 3.69 Mbar. The good quantitative agreement of the results of the empirical model and experiment demonstrates the predictive power of the model.

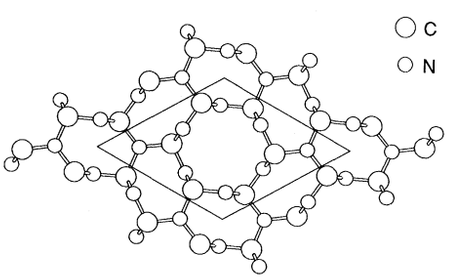


**Fig. 1.** Structure of β-$C_3N_4$ in the *a*-*b* plane. The *c*-axis is normal to the page. Half the atoms illustrated are located in the $z = -c/4$ plane, the other half are in the $z = c/4$ plane. The structure consists of these buckled planes stacked in AAA. . . sequence. The parallelogram shows the unit cell.

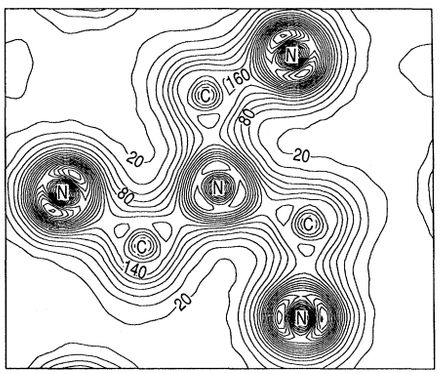


**Fig. 2.** Valence charge density of β-$C_3N_4$ in the [0001] plane. The contours are in units of electrons per cell. The contour interval is 20 electrons per cell.

Based on this model, it was suggested (*2*) that a covalent solid formed between C and N could have a larger bulk modulus than diamond. In this work, we investigate the structural and electronic properties of a solid of this type using first principles pseudopotential calculations (*5*). In choosing a candidate structure that can be used as a prototype for a covalent C-N solid, the simple zinc blende structure is ruled out because in a hypothetical zinc blende compound the first antibonding band would be occupied. This would distribute charge in antibonding regions and it is doubtful that such a structure would be stable. Instead, a more complex structure for a C-N solid, based on the known β-$Si_3N_4$ structure with C substituted for Si, is considered. The octet rule for covalent bonding is satisfied in this structure, and no antibonding states are occupied. In Fig. 1, the structure is shown to consist of buckled layers stacked in an AAA. . . sequence (*8*). The unit cell is hexagonal and contains two formula units (14 atoms) with local order such that C atoms occupy slightly distorted tetrahedral sites while N atoms sit in nearly planar triply coordinated sites. This structure can be thought of as a complex network of $CN_4$ tetrahedra that are linked at the corners. The atomic coordination suggests $sp^3$ hybrids on

Department of Physics, University of California, Berkeley, CA 94720, and Materials and Chemical Sciences Division, Lawrence Berkeley Laboratory, Berkeley, CA 94720.